IEEE Access
Multidisciplinary ⋮ Rapid Review ⋮ Open Access Journal

Received October 26, 2020, accepted November 9, 2020, date of publication November 19, 2020, date of current version December 7, 2020.

Digital Object Identifier 10.1109/ACCESS.2020.3039373

The Orthogonal Wavelets in the Frequency Domain Used for the Images Filtering

VILIAM ĎURIŠ[1], SERGEY G. CHUMAROV[2], GENNADY M. MIKHEEV[3], KONSTANTIN G. MIKHEEV[3], AND VLADIMIR I. SEMENOV[4]

[1]Department of Mathematics, Constantine the Philosopher University in Nitra, 949 74 Nitra, Slovakia
[2]Department of Radio Engineering, I. N. Ulyanov Chuvash State University, 428015 Cheboksary, Russia
[3]Udmurt Federal Research Center, Institute of Mechanics, Ural Branch of the Russian Academy of Sciences, 426067 Izhevsk, Russia
[4]Department of General Physics, I. N. Ulyanov Chuvash State University, 428015 Cheboksary, Russia

Corresponding author: Viliam Ďuriš (vduris@ukf.sk)

This work was supported by the Ministry of Education and Science of the Russian Federation under Grant AAAA-A19-119021890083-0.

ABSTRACT At present, discrete wavelet transform (Mallat algorithm) is used for signal decomposition and reconstruction. Discrete wavelets are asymmetrical, not smooth functions and do not allow decomposition of signals with a multiplicity of less than two, which limits the number of decomposition levels. Continuous wavelet transform has a number of positive properties (symmetry, smoothness of the basis function) which are necessary for signal analysis and synthesis. The article proposes algorithms for calculating direct and inverse continuous wavelet transforms in the frequency domain, which allows decomposing, reconstructing and filtering the image with high speed and accuracy. It is established that application of fast Fourier transform reduces the conversion time by four orders of magnitude in compared to direct numerical integration. The results of applying algorithms to the images obtained with an optical microscope are presented. Orthogonal symmetric and anti-symmetric wavelets with rectangular amplitude frequency response are also presented. It is shown that these firstly designed wavelets allow one to reconstruct the signal even faster than the algorithms created using fast Fourier transform. Continuous wavelet transform has been found to allow multiscale analysis of signals with a multiplicity of less than two. In addition, the construction of orthogonal wavelets in the frequency domain with the maximum possible number of zero moments allows one to analyze the finer (high-frequency) structure of the signal, as well as to suppress its slowly changing components, which makes it possible to concentrate energy in a few significant coefficients, which is a prerequisite for compression.

INDEX TERMS Algorithms, image filtering, signal analysis, wavelet transforms.

I. INTRODUCTION

Currently, in various scientific problems, the phenomenon of Raman scattering (Raman) employed in the most modern spectrometers is widely used for the study of the structure and properties of various materials. As a rule, all Raman spectrometers are equipped with built-in video cameras for outputting the image obtained with an optical microscope on the display device, which allows one to adjust the laser focus and map the sample. These tasks do not require high-resolution images, therefore, spectrometers, the high price of which is mainly due to the spectrograph, are not equipped with high-quality video cameras. Hence, images obtained with a multiple-magnification optical microscope (from 50 ×) have a low level of contrast and detail, which may be important, for example, when laser recording images on carbon nanomaterial films [1], [2]. In this regard, further digital processing of images obtained by an optical microscope is of interest in order to increase their contrast and detail. One of the methods to improve the quality of micrographs is the wavelet analysis method. The basics of wavelet analysis were developed as an alternative to the Fourier transform for the study of time (spatial) series with pronounced heterogeneity. Wavelet transforms (WTs) are usually divided into discrete and continuous WTs. The development of wavelets has various directions, which emerged in the work of Haar in the early 20th century. A significant contribution to the theory of wavelets was made by Grossman and Morlaix, who formulated the main ideas of continuous WT [3]. I. Daubechies developed orthogonal wavelets with a compact support [4].

The associate editor coordinating the review of this manuscript and approving it for publication was Hamed Azami.

Mallat proposed a multi-scale method [5]. In contrast to the Fourier transforms, which localize the frequency, but do not give a temporal resolution of the process, and from the apparatus of delta functions, which localizes time instants, but does not have a frequency resolution, a WT that has a self-adjusting movable time-frequency window identifies both low-frequency and high-frequency characteristics of the signal at different time intervals. The indicated universality of wavelet analysis leads to its widespread use in various fields of knowledge [6], [7]. Discrete WT is widely used in engineering and programming, and continuous WT - in scientific research. Families of analyzing functions called wavelets are used in the analysis of images of various nature to study the structure of turbulent fields and compress large volumes of information. WT is used to determine the characteristics of fractal objects; they are used in astrophysics, geophysics, optics, and quantum mechanics [8]–[11].

Abdulhussain *et al.* presented orthogonal polynomials with high energy compaction [12]–[14]. The amplitude-frequency characteristics of these polynomials similar to that of wavelets based on Gauss functions, while the wavelets we working with have rectangular amplitude-frequency characteristics, which is benefit.

In our work we use the concepts of time and frequency domain. If the signal is time-dependent, we are referring to the time domain. If the signal depends on a coordinate (image), we are also referring to the time domain, although it would be possible to refer to a spatial domain. In the case of a Fourier transform of a signal we move to the frequency domain, regardless of whether the signal is time-dependent or coordinate-dependent. For a time-dependent signal, in the case of a Fourier transform, we refer to the frequency of the signal. For a coordinate-dependent signal, we can refer to the spatial frequency in the Fourier transform, but for convenience we are just referring to the frequency. Thus, the signal can be described either in the time domain or in the frequency domain.

II. PRINCIPLE AND ALGORITHM OF DIRECT WAVELET TRANSFORM OF SIGNALS IN THE FREQUENCY DOMAIN

To calculate the wavelet scalogram of the signal based on the derivatives of the Gauss function, the continuous WT formula is used:

$$W(a,b) = \frac{1}{\sqrt{a}} \int_{-\infty}^{\infty} S(t)\psi\left(\frac{t-b}{a}\right) dt, \tag{1}$$

where $W(a, b)$ – wavelet scalogram if the signal, a is the scale value, b is the translational value, $S(t)$ – signal, ψ - wavelet.

A lot of time is required to calculate the WT by direct numerical integration, therefore, the wavelet scalogram is calculated in the frequency domain using the fast Fourier transform (FFT). The number of multiplication operations for direct numerical integration increases proportionally to N^2, and when switching to the frequency domain, that is, when using FFT, the number of multiplication operations increases proportionally to $N \cdot \log_2 N$. (N is the number of counts in the signal) [15]. The calculation of the wavelet spectrum is a convolution of the signal and the wavelet, therefore, when transforming Fourier convolutions the Fourier spectra of the signal and the wavelet are multiplied. In order to move from the frequency domain to the time domain, it is necessary to calculate the inverse Fourier transform of the obtained complex conjugate spectrum. Thus, in order to calculate the WT of the signal in the frequency domain, it is necessary to obtain the Fourier spectra of the signal and wavelet for different scale values a, find the complex conjugate spectrum and the inverse Fourier transform of complex conjugate spectra to obtain the wavelet scalogram of the signal.

The algorithm for the numerical calculation of the direct continuous fast WT of a signal $S(t)$ according to formula (1) in the frequency domain includes the following steps:

1. The coefficients of the trigonometric series $a_1(n), b_1(n)$ of the signal $S(k)$ are calculated using the FFT (n is a trigonometric coefficient number):

$$a_1(n) = \frac{1}{N} \sum_{k=0}^{N-1} S(k) \cos\left(\frac{2\pi nk}{N}\right), \tag{2}$$

$$b_1(n) = \frac{1}{N} \sum_{k=0}^{N-1} S(k) \sin\left(\frac{2\pi nk}{N}\right) 0 \tag{3}$$

2. The coefficients of the trigonometric series $a_2(n)$, $b_2(n)$ of the wavelet $\psi(k)$ are calculated using the FFT:

$$a_2(n) = \frac{1}{N} \sum_{k=0}^{N-1} \psi(k) \cos\left(\frac{2\pi nk}{N}\right), \tag{4}$$

$$b_2(n) = \frac{1}{N} \sum_{k=0}^{N-1} \psi(k) \sin\left(\frac{2\pi nk}{N}\right). \tag{5}$$

3. The complex conjugate spectrum is calculated:

$$c_1(n) = a_1(n) \cdot a_2(n) + b_1(n) \cdot b_2(n), \tag{6}$$

$$c_2(n) = b_1(n) \cdot a_2(n) - a_1(n) \cdot b_2(n), \tag{7}$$

where c_1 and c_2 are Fourier coefficients after multiplying the Fourier coefficients of the signal and wavelet.

Most continuous wavelets are either even or odd functions. For even wavelets, the series is composed of cosines alone, and for odd ones, it is composed of sine functions only. For even wavelets, $b_2(n) = 0$ and

$$c_1(n) = a_1(n) \cdot a_2(n), \tag{8}$$

$$c_2(n) = b_1(n) \cdot a_2(n). \tag{9}$$

For odd wavelets, $a_2(n) = 0$ and

$$c_1(n) = b_1(n) \cdot b_2(n), \tag{10}$$

$$c_2(n) = -a_1(n) \cdot b_2(n). \tag{11}$$

The wavelet spectrum $W(a, b)$ (the matrix of wavelet coefficients $M \times N$) for the input analyzed signal with a length of N samples is obtained by calculating M inverse Fourier

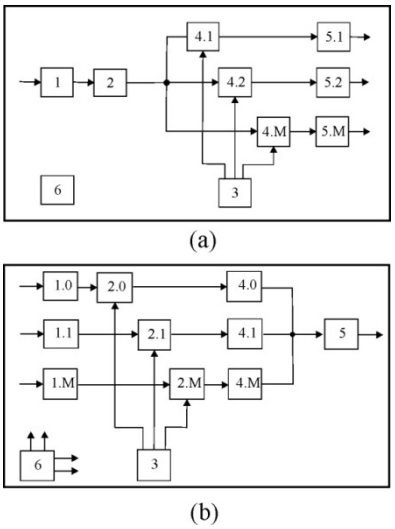

FIGURE 1. **(a) The structural diagrams of the direct fast wavelet transform: 1 – analog-to-digital converter (ADC); 2 – FFT calculator; 3 – read-only memory; 4.1 - 4.M – multipliers; 5.1 - 5.M – inverse FFT calculators; 6 – control device. (b) The structural diagram of the inverse wavelet transform: 1.0 - 1.M – FFT calculators; 2.0 - 2.M – multipliers; 3 – read-only memory; 4.0 - 4.ì – inverse FFT calculators; 5 – adder; 6 – control device.**

transforms from the complex conjugate spectrum using the formula:

$$W(a,b) = \sum_{k=0}^{N-1} (c_1(k) + ic_2(k)) \exp\left(i\frac{2\pi nk}{N}\right). \quad (12)$$

Here M is the number of levels of decomposition (decomposition) of a signal with a length of N samples. M levels of wavelet coefficients with length N are formed, so the total number of wavelet coefficients is $M \times N$. A certain individual coefficient at the M level, for example, at the point n ($1 <= n <= N$), is obtained by the inverse Fourier transform of the complex-conjugate spectrum. The scale factor is different at each level.

The block diagram of the direct fast continuous WT is shown in Fig. 1a. The analyzed signal $S(t)$ is fed to the ADC (block 1), from the output of which a discrete sample $S(n)$ with the length of N subsamples is fed to the input of the FFT calculator (block 2).

From the output of block 2, the coefficients of the series $a_1(n)$, $b_1(n)$ of the signal simultaneously arrive at the first inputs of M multipliers (blocks 4.1 - 4.M). From the ROM (block 3), the coefficients of the series $a_2(n)$ (for even ones), $b_2(n)$ (for odd) wavelets arrive at the second inputs of the M multipliers (blocks 4.1 - 4.M), from the outputs of which the multiplication results go to the inputs of the inverse FFT calculators (blocks 5.1 - 5.M). The results of the WT of the signal are taken from the outputs of M inverse FFT calculators (blocks 5.1 - 5.M) in the form of an array of values of wavelet coefficients of size M scales by N shifts $W(m,n)$. The control device (block 6) synchronizes the operation of ADC blocks (block 1), FFT calculators (block 2), multipliers (blocks 4.1 - 4.M), and inverse FFT calculators (blocks 5.1 - 5.M). This device allows you to select various types of wavelet functions with an arbitrary step of discretization of scale factors stored in ROM (block 3) for analysis of the input signal [16]–[18].

III. PRINCIPLE AND ALGORITHM OF THE INVERSE WAVELET TRANSFORM OF SIGNALS IN THE FREQUENCY DOMAIN

Signal reconstruction is performed using the inverse continuous WT formula:

$$S(t) = C_\psi^{-1} \int_0^\infty \int_{-\infty}^\infty \psi\left(\frac{t-b}{a}\right) W(a,b) \frac{da \cdot db}{a^{3+k}}, \quad (13)$$

where C_ψ is the normalizing coefficient:

$$C_\psi = \int_{-\infty}^\infty |F_\psi(\omega)|^2 \cdot \omega^{-1} d\omega < \infty,$$

$F_\psi(\omega)$ is the Fourier spectrum of the basis function, ω is the cyclic frequency, k is the exponent of the scale factor.

Calculation of WT by direct numerical integration (i.e. direct and inverse WT in the time domain) for long time sequences using formula (13) takes a significant amount of time to complete. Hence, to increase performance, the authors developed an algorithm for continuous fast WT in the frequency domain using the FFT. The normalizing coefficient in the formula (13) of the continuous inverse wavelet transform $C = C_\psi$ in the developed algorithm is calculated from the analog of the Parseval theorem for wavelet coefficients [19]:

$$\int S(t) S^*(t)\, dt = C^{-1} \iint W(a,b) W^*(a,b) \frac{dadb}{a^2} \quad (14)$$

After determining the normalizing coefficient C from (14), it is substituted into the formula

$$S(t) = C^{-1} \int_0^\infty \int_{-\infty}^\infty \psi\left(\frac{t-b}{a}\right) W(a,b) \frac{dadb}{a^2}. \quad (15)$$

The theoretical basis for calculating the inverse continuous fast wavelet transform of the signal $S(t)$ in the frequency domain is the use of formulas (14) and (15). The inverse transformation of the product of the spectra of the wavelet spectrum $W(a,b)$ and the wavelet $\psi(t)$ is used to calculate the integral over the variable b. The reconstructed signal $S(t)$ is calculated by summation of the obtained integral over the scale value a.

The algorithm for calculation of the inverse continuous wavelet transform using formula (13) in the frequency domain includes the following steps.

1. The coefficients of the trigonometric series $d_1(n)$ of the wavelet scalogram $W(a,b)$ are calculated using the direct FFT according to the formula:

$$d_1(n) = \frac{1}{n} \sum_{k=0}^{N-1} W(a,k) \cos\left(\frac{2\pi nk}{N}\right). \quad (16)$$

2. The coefficients of the trigonometric series $e_1(n)$ of the wavelet scalogram $W(a,b)$ are calculated using the direct

FFT according to the formula:

$$e_1(n) = \frac{1}{n}\sum_{k=0}^{N-1} W(a,k)\sin\left(\frac{2\pi nk}{N}\right). \quad (17)$$

3. The coefficients of the trigonometric series $d_2(n)$ of the wavelet $\psi(t)$ are calculated using the direct FFT according to the formula:

$$d_2(n) = \frac{1}{n}\sum_{k=0}^{N-1} \psi(k)\cos\left(\frac{2\pi nk}{N}\right). \quad (18)$$

4. The coefficients of the trigonometric series $e_2(n)$ of the wavelet $\psi(t)$ are calculated using the direct FFT according to the formula:

$$e_2(n) = \frac{1}{n}\sum_{k=0}^{N-1} \psi(k)\sin\left(\frac{2\pi nk}{N}\right). \quad (19)$$

5. The complex conjugate spectrum is calculated using the formulas

$$f_1(n) = d_1(n)\cdot d_2(n) + e_1(n)\cdot e_2(n), \quad (20)$$
$$f_2(n) = e_1(n)\cdot d_2(n) - d_1(n)\cdot e_2(n). \quad (21)$$

For an even wavelet, the series is made up of single cosines, and for an odd one - of single sinuses.

For an even wavelet $e_2(n) = 0$ and

$$f_1(n) = d_1(n)\cdot d_2(n), \quad (22)$$
$$f_2(n) = e_1(n)\cdot d_2(n). \quad (23)$$

For and odd wavelet $d_2(n) = 0$ and

$$f_1(n) = e_1(n)\cdot e_2(n), \quad (24)$$
$$f_2(n) = -d_1(n)\cdot e_2(n). \quad (25)$$

6. For an even wavelet the function s'_m is calculated using $M+1$ inverse Fourier transforms of the complex conjugate spectrum (22), (23):

$$s'_m(n) = \sum_{k=0}^{N-1}(f_1(k) + if_2(k))\exp\left(i\frac{2\pi nk}{N}\right). \quad (26)$$

7. For an odd wavelet the function s'_m is calculated using $M+1$ inverse Fourier transforms of the complex conjugate spectrum (24), (25):

$$s'_m(n) = \sum_{k=0}^{N-1}(f_1(k) + if_2(k))\exp\left(i\frac{2\pi nk}{N}\right), \quad (27)$$

the notation' does not mean differentiation.

8. The normalizing coefficient C is calculated using the formula (14).

9. The signal is reconstructed according to the formula:

$$S(n) = C\sum_{m=0}^{m} s'_m(n), \quad (28)$$

where m is the level of decomposition.

The block diagram of the inverse continuous WT device is shown in Fig.1b.

The wavelet spectrum $W(m,n)$ is sent to the inputs of the FFT calculators (blocks 1.0 - 1.M), from the output of which the series $d_1(n)$, $e_1(n)$ coefficients simultaneously arrive at the first inputs of the $M+1$ multipliers (blocks 2.0 - 2.M). From the ROM (block 3), the coefficients of the series $d_2(n)$ (for even), $e_2(n)$ (for odd) wavelets arrive at the second inputs of $M+1$ multipliers (blocks 2.0 - 2.M), from the outputs of which the multiplication results go to the inputs of the inverse FFT calculators (blocks 4.0 - 4.M). From the M outputs of the inverse FFT calculators (blocks 4.0 - 4.M), they are fed to the inputs of the adder (block 5), where the results of the inverse WT are added together, from the output of which the result of the inverse WT signal $S(n)$ is taken. The control device (block 6) synchronizes the operation of blocks of FFT calculators (blocks 1.0 - 1.M), multipliers (blocks 2.0 - 2.M), inverse FFT calculators (blocks 4.0 - 0.M) and the adder (block 5) [16], [17], [20].

IV. MULTI-SCALE ANALYSIS OF ONE-DIMENSIONAL AND TWO-DIMENSIONAL SIGNALS

The concept of multiresolution analysis (MRA) is fundamental in the theory of wavelets. QMA allows one to decompose an arbitrary signal $s(t)$ into many different-scale functions, the combination of which gives the original signal $s(t)$, or approximates the signal with a certain accuracy depending on the number of values of the scaling coefficient m. If the value of m is small, the approximation is rough and lacking the level of details. With an increase in values of m, the accuracy of approximation increases.

Compact support wavelets are currently used for MRA. These include orthogonal wavelets of Dobeshi (dbN), Simlet (symN), Koiflet (coifN), and biorthogonal B-spline wavelets (biorNr), (rbioNr). The main disadvantage of these wavelets is that they are asymmetric and non-smooth functions that do not have an analytical representation. A fast wavelet transform algorithm (Mallat algorithm) is used for MRA, as follows.

First, the signal is passed through a low-frequency filter with a pulse response g, i.e. convolution is calculated. Also, the signal is decomposed using a high-frequency filter h. The result is detail coefficients (after the high-frequency filter) and approximation coefficients (after the low-frequency filter). These two filters are interconnected and are called quadrature mirror filters. Since half of the frequency range of the signal was filtered out, according to Kotelnikov's theorem, the signal readings can be thinned by a factor of two. This will halve the time resolution due to signal thinning. However, each of the resulting signals represents half the frequency band of the original signal, so that the frequency resolution is doubled. This process can be repeated several times to further increase the frequency resolution with further thinning of the coefficients after low-frequency and high-frequency filtering.

This decomposition can be represented in the form of a binary tree, where the leaves and nodes correspond to spaces with different time-frequency localization. This tree represents the structure of the bank (comb) of filters. At each level, the signal is decomposed into low and high frequencies. After double decimation, the signal length should be a multiple of $2n$, where n is the number of decomposition levels. Signal

recovery occurs in the reverse order, i.e., zero elements are added to the detail and approximation coefficients, passed through mirror filters, and added.

For many applications, discrete two-dimensional WT is used in a construction where the wavelet bases are obtained by the tensor product of two one-dimensional multiresolution analyzes by columns and by rows. There are a standard and a non-standard construction of a two-dimensional basis. The standard construction of a two-dimensional basis of wavelets consists of taking all kinds of tensor products of functions of a one-dimensional basis. For standard image decomposition, one-dimensional conversion of all rows, and then all columns, is necessary. With the non-standard construction of a two-dimensional basis, one scaling function and three wavelets are formed, called horizontal, vertical, and diagonal. In this design, low- and high-pass filtering is repeated across rows and columns by applying all four possible combinations. Discrete WT for a non-standard two-dimensional basis is defined by the scheme

$$z \to \{H_r H_c z, H_r G_c z, G_r H_c z, G_r G_c z\}, \tag{29}$$

where H is the low-frequency filtering, G - high-frequency filtering.

The index r means that the filter is applied to the rows, and the index c means that it is applied to the columns. If the signal (image) is given by an array of $N \times N$ elements, then each array of approximation and detail (for horizontal, vertical, and diagonal wavelet) coefficients of the first level consists of $N/2 \times N/2$ elements. For the second level - $N/4 \times N/4$ elements, for the third level - $N/8 \times N/8$ elements, etc. Signal decomposition into wavelet series at a given resolution level m is performed using these coefficients [21]–[24].

V. MULTIRESOLUTION IMAGE ANALYSIS USING WAVELETS BASED ON DERIVATIVES OF THE GAUSS FUNCTION IN THE FREQUENCY DOMAIN

At present, the MRA of signals is performed using discrete orthogonal wavelets. It is noted in the scientific literature that analysis is not orthogonal for continuous WT, wavelets do not have a compact support, there is no scaling function, and reconstruction is not guaranteed. In this regard, the compression and filtering of signals are performed using discrete wavelets.

Continuous WT is used to analyze and study signals, since the transitions between scale coefficients can be arbitrarily small [3]–[5], [8]–[11], [15], [21]–[33]. All discrete wavelets are constructed in the time domain. To obtain such wavelets, a system of equations is solved so that the wavelets have zero moments of the nth order. Since wavelets are constructed in the time domain, their frequency characteristics are far from ideal filters. For example, these wavelets are asymmetric and non-smooth functions; therefore, their phase-frequency characteristics are not linear. The nonlinearity of the phase characteristic leads to signal distortion; therefore, biorthogonal wavelets are used to compensate for distortions. That is, decomposition is performed with one wavelet, and reconstruction with another wavelet. In the JPEG-2000 photo compression scheme, the 9/7 biorthogonal transformation is applied.

The authors developed the MRA algorithm using wavelets based on derivatives of the Gauss function. The main advantage of these wavelets is that they are smooth and symmetric functions having derivatives of N-order. Such functions are necessary for WT.

The forward and reverse fast continuous WT algorithms developed in this work allow any signal to be represented as

$$S(t) = \sum_{m=0}^{m} s_m(t), \tag{30}$$

where $s_m(t) = Cs'_m(t)$.

The constant C can be defined more simply using the corollary of formula (14) (Parseval's theorem). In the space of real functions, the signal energy density characterizing the signal energy density as a function of scale factor a at a moment of time b is as follows:

$$E_W(a, b) = W_l^2(a, b). \tag{31}$$

The local energy density at point $b = t_0$

$$E_\delta(a, t_0) = W_l^2(a, t_0). \tag{32}$$

Then

$$S(t_0) = C \sum_{m=0}^{m} s'_m(t_0). \tag{33}$$

The constant C calculated using the formula (14) coincides with the constant found by the formula (33). So that when calculating by formula (33) there is no division by zero or multiplication by a negative number, it is better to calculate the constant C for the function at maximum.

When performing MRA with a discrete WT, the signal space $L^2(R)$ is represented as a system of nested subspaces W_m. By analogy with a discrete WT, the developed reverse WT algorithm allows the entire signal space $L^2(R)$ to be represented as a sequence of closed nested subspaces in one another:

$$\ldots \subset W_m \subset W_{m-1} \subset \ldots W_0.$$

The ''sizes'' of subspaces continuously expand as the value of m decreases, and the union of all subspaces, at the limit, gives the space $L^2(R)$.

We form functions $s''_m(t)$ from $s_m(t)$ such that (the symbol$''$ does not mean double differentiation):

$$s''_m(t) = s_m(t), s''_{m-1}(t) = s''_m(t) + s_{m-1}(t),$$

and so on.

If the signal $s''_{m-1}(t)$ belongs to the space W_{m-1}, then at the same time it is in the space W_m, along with it the signal $s''_m(t)$. A decrease in the number of the space allows us to study smaller and smaller details and features of the signal with higher-frequency components, i.e. move from a rough approximation to a higher resolution approximation. Then the signal with the largest time resolution $S(t) = s''_0(t)$.

The variable m is called the same as a, the scale coefficient, or level of analysis.

If the value of m is large, then the function is a rough approximation of $S(t)$, lacking in the level of detail. With a decrease of m, the accuracy of approximation increases. In the literature on discrete WT, an m-step discrete WT is called MRA. The maximum value of m is called the decomposition depth of the signal. Compared with MRA signals using discrete wavelets, MRA in the frequency domain allows one to decompose the signal into a larger number of levels, since the multiplicity of the analysis can be less than two [31], [32]. Since with a discrete WT, the scale factor is two, the decomposition depth m is limited by the signal duration, as the base two logarithm of the sample size. For MRA in the frequency domain, the scale factor can range from one to two and have a fractional value. The smaller this coefficient, the greater the depth of decomposition [16]–[18], [20].

In this case, the WT is carried out for the entire image, a sawtooth-like scan along rows and columns. Unlike the Mallat algorithm, this algorithm allows one to get much more levels of decomposition, thereby allowing to examine the image in more detail, and the quality factor of wavelets increases. Also, when using this algorithm, the mosaic does not appear when approximating the image with high-level coefficients. The peculiarity of using this algorithm is that it is possible to construct wavelets in the frequency domain without the use of multiplications.

Thus, the conversion takes several times less time than the conversion with the use of wavelets based on derivatives of the Gauss function. The WT time decreases by a factor of several tens of thousands compared with direct numerical integration for a large sample length of the signal. In fact, for the algorithm we have developed, there are no approximation and detail coefficients, but there are decomposition levels corresponding to the decomposition levels in the Mallat algorithm and we can compare the results of the decompositions. Although the conversion time in the Mallat algorithm is almost the same as the algorithm in the frequency domain, the quality is much worse. Reconstruction of an image with detailed coefficients when using the algorithm in the frequency domain gives a sharper image than in the MATLAB numerical and symbolic computing environment.

VI. USE OF WAVELET ANALYSIS TO IMPROVE THE QUALITY OF IMAGES OBTAINED USING OPTICAL MICROSCOPES

Figure 2 shows a diagram of an experiment on laser recording of images and outputting the images to a video camera, performed using a Raman spectrometer Horiba HR800. Laser image recording was carried out on a single-walled carbon nanotube (SWCNT) film (10) on a substrate of polyethylene terephthalate (11) (see Fig.2, b). SWCNT film (10) was irradiated by laser radiation (1) at a wavelength of 633 nm passing through a mirror (2) and focused by a 50 × objective (3) (see Fig. 2, a). The optical axis of the objective (3) is perpendicular to the surface of the film (10) located in the

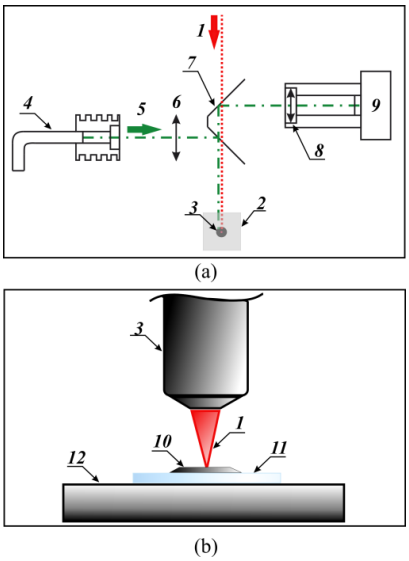

FIGURE 2. The experimental design for laser recording of images and the output of this images on the screen from (a) above and (b) in profile. *1* – laser beam; *2* - a mirror; *3* - a 50 × objective; *4* - optical fiber for illuminating the sample with white light; *5* - the optical path of the light flux from the fiber optic irradiator; *6, 8* - lenses; *7* - two kinematic beam splitters; *9* - video camera; *10* - single-walled carbon nanotube film; *11* - the film substrate; *12* - coordinate table.

horizontal plane (see Fig. 2, b). To observe the sample using a video camera (9), two 50/50 beam splitters (7) are installed. The first receives the light flux from the fiber optic irradiator (4) passing through the lens (6) and directs it to the sample. The second directs the image of the sample to the video camera (9) through the lens (8). It should be noted that the quality of video camera (9), built into the Horiba HR800 Raman spectrometer, does not allow to get the image of high contrast and detail level using objectives 50 × or higher. During the experiments, it was shown that a short-term laser exposure to the film is accompanied by the appearance of a brightened point on the irradiated surface. With continuous exposure to laser radiation and moving the film (10) in the horizontal plane using the coordinate table (12) relative to the laser beam focused by the objective (3), it was possible to obtain a solid line of bleaching.

Fig. 3,a shows a 512 × 512 pixels black-and-white image of two lines on an SWCNT film obtained this way. As noted above, the video camera that displays the image on the screen of the monitor has a low level of contrast and detail, therefore, the lines obtained during laser recording are not clearly visible in the presented image. To obtain a better image, the wavelet analysis method was used. The filtration process was performed by suppressing low-frequency components of the Fourier spectrum. That is, decomposition levels were removed, which is equivalent to zeroing of low-frequency components of the Fourier spectrum. Figure 3,b shows the reconstructed image using coefficients of 1-9 levels. It is seen that after the wavelet analysis of the image, the lines, obtained by laser recording are clearly visible, and even the small inclusions present on the SWCNT film became noticeable. Thus, the reconstruction of images obtained by an

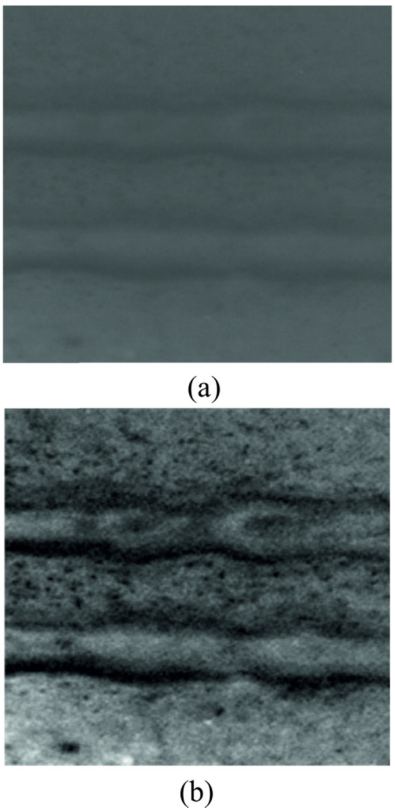

FIGURE 3. Image obtained by (a) an optical microscope and (b) its reconstruction using coefficients of 1–9 levels.

optical microscope with various coefficients and a subsequent increase in contrast can improve the quality of the obtained image [18].

VII. CONSTRUCTION OF ORTHOGONAL SYMMETRIC AND ANTISYMMETRIC WAVELETS IN THE FREQUENCY DOMAIN

As with the Fourier transform, the signal can be expanded in cosines and sines, so the signal can be expanded in terms of the wavelet basis. For this to take place, wavelets must be orthogonal. The family of wavelet functions $\psi_{ab}(t)$ is generated from a single "mother" function $\varphi(t)$ by means of expansion (compression) and shift

$$\psi(t) = \frac{1}{\sqrt{a}}\varphi\left(\frac{t-b}{a}\right), \tag{34}$$

where a is the scale value, b is the translational value. For given values of the parameters a and b, the function $\psi_{ab}(t)$ is the wavelet. The main features of wavelets are boundedness, localization, self-similarity, and zero mean. A zero mean means that the graph of the function must oscillate (have an alternating sign) around zero on the time axis and have zero area

$$\int_{-\infty}^{\infty} \psi(t)\, dt = 0. \tag{35}$$

The area of the function $\psi(t)$ is equal to zero, i.e. zero moment, which leads to the fact that the Fourier transform

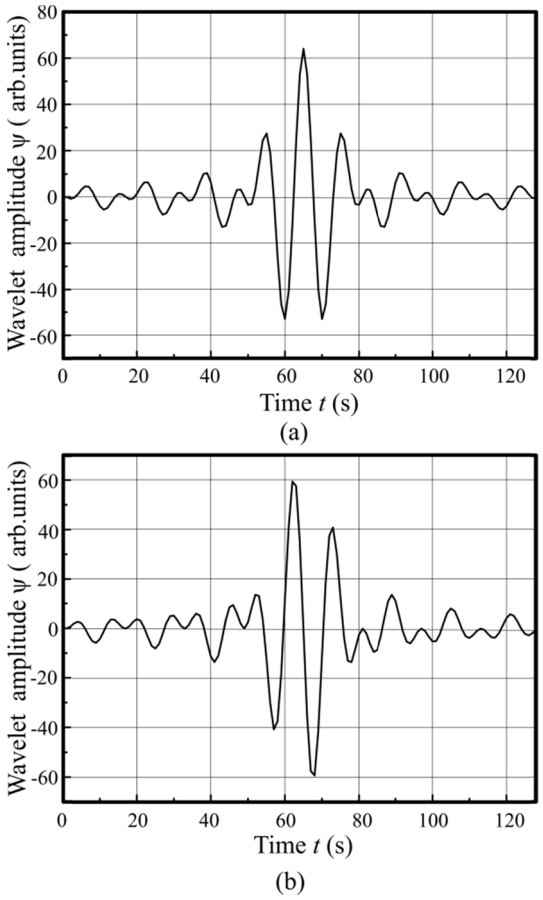

FIGURE 4. (a) Symmetric orthogonal wavelet and (b) antisymmetric wavelet.

$S(\omega)$ of this function is equal to zero at $\omega = 0$ and has the form of a band-pass filter. For various values of the scale factor a, it is a set of bandpass filters. It is often necessary for applications that all the first n moments are equal to zero:

$$\int_{-\infty}^{\infty} t^n \psi(t)\, dt = 0. \tag{36}$$

Wavelets of nth-order allow one to analyze a finer (high-frequency) signal structure, suppressing its slowly changing components [4]–[8]. According to the literature, it is desirable to have orthogonal symmetric and antisymmetric wavelets to study signals; however, ideal wavelets like that do not exist. In this regard, the construction of wavelets in the frequency domain with the maximum possible number of zero moments is relevant. Since orthogonal wavelets are constructed in the frequency domain, the resulting wavelets have almost ideal amplitude-frequency characteristics and linear phase-frequency characteristics. Almost ideal in the sense that they differ from theoretical characteristics only in the calculation error.

Fig. 4 illustrates a symmetric and antisymmetric orthogonal wavelets in the time domain constructed in the frequency domain. It shows that the wavelets have many maximal and minimal values. There are even more of them, since only fifth of the wavelets is shown in the figures. To obtain such

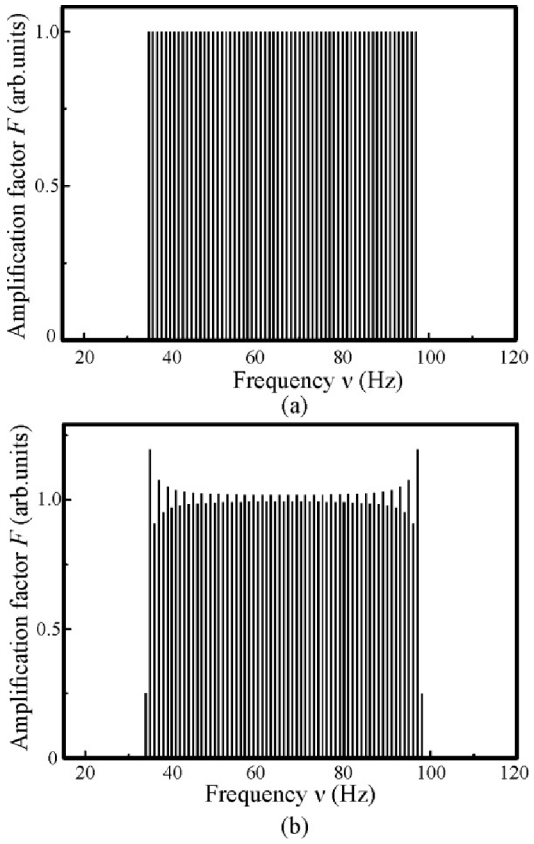

FIGURE 5. (a) Frequency-amplitude property of an orthogonal wavelet; (b) Frequency-amplitude property of a wavelet constructed in the time domain.

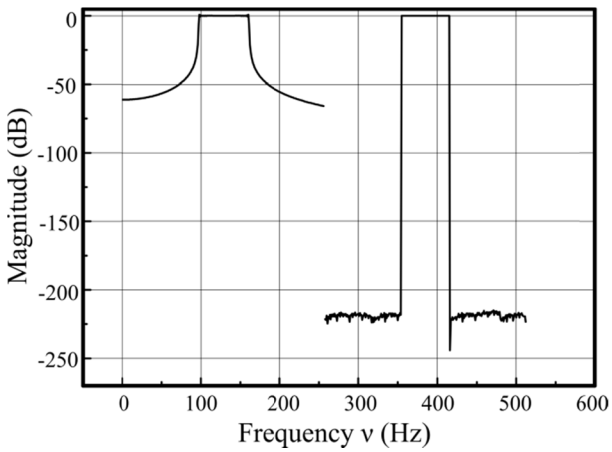

FIGURE 6. Frequency response of a wavelet constructed in the time domain and in the frequency domain.

wavelets in the time domain using Mallat algorithm, it would be necessary to solve equations with the same amount of maximal and minimal values for each level of decomposition.

Fig. 5,a shows the amplitude-frequency property of an antisymmetric orthogonal wavelet ν (ν is frequency). There is no unevenness in the pass band or in the stop band and there is no transition band. Fig. 5,b shows the amplitude-frequency response of a wavelet constructed in the time domain. The wavelet equation has the form:

$$\psi\left(t,a,b\right)=\frac{\sin\left(\frac{t-b}{a}\right)}{\left(\frac{t-b}{a}\right)}\cos\left(\omega t\right). \tag{37}$$

Fig. 5,b shows that in the passband the amplitude-frequency characteristic is uneven. This effect is called the Gibbs phenomenon. It was first studied in connection with the truncation of the Fourier series used to decompose the harmonics of periodic signals.

Fig. 6 shows the frequency response of the wavelet constructed in the time domain (Fig. 5,b) and the frequency response of the orthogonal wavelet constructed in the frequency domain (Fig. 5,a) on the same graph in decibels. Up to a frequency of 260 units, the frequency response of a wavelet constructed in the time domain is presented, and from 260 to 512, a wavelet constructed in the frequency domain is presented. Fig. 6 clearly shows how much the frequency characteristics of these wavelets differ when comparing them on the same scale. The amplitude-frequency characteristic of the wavelet constructed in the frequency domain can be considered ideal, since the signal is attenuated by a factor of a billion trillions in stop band.

VIII. CONCLUSION

Wavelets based on derivatives of the Gauss function allow us to reconstruct a signal, perform a multiresolution analysis, filtering one-dimensional and two-dimensional signals. Pearson's correlation coefficient is higher than 0.999. The profiling of the program shows that the wavelet transform time using the FFT is 15,000 times lesser than with direct numerical integration for 32768 samples of the signal. Studies show that MRA using continuous wavelets is better than MRA using discrete wavelets, since discrete wavelets are not symmetrical functions, therefore, they have a non-linear phase-frequency characteristic.

Orthogonal wavelets constructed in the frequency domain can reduce the time of decomposition and reconstruction of one-dimensional and two-dimensional signals, since it is not necessary to calculate the Fourier spectra of wavelets. They are formed in the frequency domain. They also allow one-dimensional and two-dimensional signals to be reconstructed with greater accuracy. Unlike the Mallat [5] algorithm, which is used for discrete WT, this algorithm allows one to obtain much more decomposition levels, that is, with a multiplicity of less than two, thereby allowing a more detailed investigation, filtering of the signal, i.e., the quality factor of wavelets increases. The construction of wavelets with a large number of zero moments allows more efficient concentration of information in the signal in fewer significant coefficients. This concentration mechanism is the main prerequisite for signal compression. The amplitude-frequency characteristics of the orthogonal symmetric and antisymmetric wavelets are ideal, in order to obtain such characteristics in the time domain it is necessary to solve a system of an infinite number of equations. And this will lead to the fact that the calculation

time of such equations will increase significantly and will lead to an increase in the calculation error.

Wavelets obtained in the frequency domain, not only have an ideal amplitude-frequency response, but also reduce the time of the WT, because there is no need to calculate some steps in the algorithm. In direct continuous WT calculation time is reduced by more than 2 times compared to the use of wavelets based on Gauss function derivatives in the frequency domain. In the reverse continuous calculation of WT the calculation time is reduced by 3 orders of magnitude for a large sample of signal in comparison with the use of wavelets based on Gauss function derivatives in the frequency domain.

ACKNOWLEDGMENT

This study was performed using equipment of the Shared Use Center "Center of Physical and Physicochemical Methods of Analysis and Study of the Properties and Surface Characteristics of Nanostructures, Materials, and Products" UdmFRC UB RAS.

REFERENCES

[1] G. M. Mikheev, K. G. Mikheev, T. N. Mogileva, A. P. Puzyr, and V. S. Bondar, "Laser image recording on detonation nanodiamond films," *Quantum Electron.*, vol. 44, no. 1, pp. 1–3, Jan. 2014.

[2] K. G. Mikheev, T. N. Mogileva, A. E. Fateev, N. A. Nunn, O. A. Shenderova, and G. M. Mikheev, "Low-power laser graphitization of high pressure—High temperature nanodiamond films," *Appl. Sci.*, vol. 10, no. 9, p. 3329, May 2020.

[3] A. Grossmann and J. Morlet, "Decomposition of hardy functions into square integrable wavelets of constant shape," *SIAM J. Math. Anal.*, vol. 15, no. 4, pp. 723–736, Jul. 1984.

[4] I. Daubechies, *Ten Lectures on Wavelets*. Philadelphia, PA, USA: Society for Industrial and Applied Mathematics, 1992.

[5] S. G. Mallat, "A theory for multiresolution signal decomposition: The wavelet representation," *IEEE Trans. Pattern Anal. Mach. Intell.*, vol. 11, no. 7, pp. 674–693, Jul. 1989.

[6] S. Glowinski, A. Blazejewski, and T. Krzyzynski, "Inertial sensors and wavelets analysis as a tool for pathological gait identification," in *Innovations in Biomedical Engineering* (Advances in Intelligent Systems and Computing), vol. 526. Cham, Switzerland: Springer-Verlag, 2017, pp. 106–114.

[7] A. Błażejewski, S. Głowiński, and I. Maciejewski, "The wavelet transfer function of a human body–seat system," *J. Low Freq. Noise, Vib. Act. Control*, vol. 38, no. 2, pp. 817–825, Jun. 2019.

[8] I. M. Dremin, O. V. Ivanov, and V. A. Nechitailo, "Wavelets and their uses," *Physics-Uspekhi*, vol. 44, no. 5, pp. 447–478, May 2001.

[9] G.-G. Stark, *The Use of Wavelets for DSP*. Moscow, Russia: Technospere, 2007.

[10] I. Y. Novikov, V. Y. Protasov, and M. A. Skopina, *Surge Theory*. Moscow, Russia: Fizmatlit, 2005.

[11] A. N. Yakovlev, *Basics of Wavelets Transform*. Moscow, Russia: Science Press, 2003.

[12] S. H. Abdulhussain, A. R. Ramli, B. M. Mahmmod, M. I. Saripan, S. A. R. Al-Haddad, and W. A. Jassim, "A new hybrid form of krawtchouk and tchebichef polynomials: Design and application," *J. Math. Imag. Vis.*, vol. 61, no. 4, pp. 555–570, May 2019.

[13] A. M. Abdul-Hadi, S. H. Abdulhussain, and B. M. Mahmmod, "On the computational aspects of charlier polynomials," *Cogent Eng.*, vol. 7, no. 1, Jan. 2020, Art. no. 1763553.

[14] B. M. Mahmmod, A. M. Abdul-Hadi, S. H. Abdulhussain, and A. Hussien, "On computational aspects of krawtchouk polynomials for high orders," *J. Imag.*, vol. 6, no. 8, p. 81, Aug. 2020.

[15] H. J. Nussbaumer, *Fast Fourier Transform and Convolution Algorithms*, vol. 2. Berlin, Germany: Springer, 1981.

[16] V. I. Semenov, "Certificate of official registration of a computer program no. 2007615024," Dept. Gen. Phys., Chuvash State Univ., Cheboksary, Russia, Tech. Rep. 2007615024, 2007.

[17] V. I. Semenov and P. V. Zheltov, "The way to recognize key words in continuous speech," Dept. Gen. Phys., Chuvash State Univ., Cheboksary, Russia, Tech. Rep. 2403628, 2008.

[18] V. I. Semenov, K. G. Mikheev, A. K. Shurbin, and G. M. Mikheev, "Filtration of images obtained by optical microscope using multiresolution analysis," *Khim. Fiz. Mezoskopiya*, vol. 16, no. 3, pp. 399–404, 2014.

[19] N. M. Astaf'eva, "Wavelet analysis: Basic theory and some applications," *Phys.-Uspekhi*, vol. 39, no. 11, pp. 1085–1108, Nov. 1996.

[20] V. I. Semenov, K. G. Mikheev, A. K. Shurbin, and G. M. Mikheev, "Construction of orthogonal wavelets in the frequency region for a multiscale signal analysis," *Khim. Fiz. Mezoskopiya*, vol. 20, no. 2, pp. 230–238, 2018.

[21] S. V. Umnyashkin, *Theoretical Foundations of Digital Signal Processing and Representation*. Moscow, Russia: Radio and Communications, 2008.

[22] E. J. Stollnitz, T. D. Derose, and D. H. Salesin, "Wavelets for computer graphics: A primer," *IEEE Comput. Graph. Appl.*, vol. 15, no. 3, pp. 76–84, May 1994.

[23] P. Singh, "Wavelet transform in image processing: Denoising, segmentation and compression of digital images," *Int. J. Sci. Res. Sci. Eng. Technol.*, vol. 2, no. 2, pp. 1137–1140, 2016.

[24] M. M. Ameen, A. Eleyan, and G. Eleyan, "Wavelet transform based face recognition using SURF descriptors," *Int. J. Electron. Electr. Eng.*, vol. 5, no. 1, pp. 94–98, 2017.

[25] M. T. Naseer and S. Asim, "Application of instantaneous spectral analysis and acoustic impedance wedge modeling for imaging the thin beds and fluids of fluvial sand systems of indus basin, Pakistan," *J. Earth Syst. Sci.*, vol. 127, no. 7, p. 97, Oct. 2018.

[26] Z. Liu, H. Chen, K. Sun, C. He, and B. Wu, "Full non-contact laser-based Lamb waves phased array inspection of aluminum plate," *J. Vis.*, vol. 21, no. 5, pp. 751–761, Oct. 2018.

[27] O. Alpar, "Online signature verification by continuous wavelet transformation of speed signals," *Expert Syst. Appl.*, vol. 104, pp. 33–42, Aug. 2018.

[28] X. Xu, M. Luo, Z. Tan, and R. Pei, "Echo signal extraction method of laser radar based on improved singular value decomposition and wavelet threshold denoising," *Infr. Phys. Technol.*, vol. 92, pp. 327–335, Aug. 2018.

[29] D. Li, T. Cheng, M. Jia, K. Zhou, N. Lu, X. Yao, Y. Tian, Y. Zhu, and W. Cao, "PROCWT: Coupling PROSPECT with continuous wavelet transform to improve the retrieval of foliar chemistry from leaf bidirectional reflectance spectra," *Remote Sens. Environ.*, vol. 206, pp. 1–14, Mar. 2018.

[30] A. Yadav, N. Sengar, A. Issac, and M. K. Dutta, "Image processing based acrylamide detection from fried potato chip images using continuous wavelet transform," *Comput. Electron. Agricult.*, vol. 145, pp. 349–362, Feb. 2018.

[31] Y. Zheng and A. Rinoshika, "Analysis of particle dynamics in a horizontal pneumatic conveying of the minimum pressure drop based on POD and wavelet transform," *Powder Technol.*, vol. 320, pp. 726–738, Oct. 2017.

[32] E. B. Postnikov, E. S. Stiukhina, and D. E. Postnov, "A fast memory-saving method for the Morlet wavelet-based transform and its application to *in vivo* assessment of microcirculation dynamics," *Appl. Math. Comput.*, vol. 305, pp. 251–261, Jul. 2017.

[33] P. Joshi, S. Prakash, and S. Rawat, "Continuous wavelet transform-based no-reference quality assessment of deblocked images," *Vis. Comput.*, vol. 34, no. 12, pp. 1739–1748, Dec. 2018.

VILIAM ĎURIŠ received the degree in mathematics and computer science. He has been an Assistant Professor with the Department of Mathematics, Faculty of Natural Sciences, Constantine the Philosopher University, Nitra, Slovakia, since 2009, focusing mainly on object programming, applied mathematics, and numerical mathematics. He is also a Founding Member of the GeoGebra Institute, Nitra, which is a part of a network of local GeoGebra institutes accredited by the International GeoGebra Institute and the Author of the local GeoGebra portal. He runs his IT projects worldwide in information technology and a professional database programmer as an Expert. He has authored many major projects and training systems. He has also been involved in major national and international projects or projects of the European Social Fund. He has received awards several times during his work at Constantine the Philosopher University, Nitra, for publishing and scientific work. He was a member of the program and organizing committee of international conferences Mathematical Conference in Nitra and Statistical Days in Nitra with the Faculty of Natural Sciences, Constantine the Philosopher University, Nitra, for seven years.

SERGEY G. CHUMAROV received the degree and the Ph.D. degree in radio engineering from Mari State Technical University, Yoshkar-Ola, Russia, in 1999 and 2002, respectively.

Since 1999, he has been with the Department of Radio Engineering and Telecommunications, I. N. Ulianov Chuvash State University, where he is currently an Associate Professor. His current research interests include radio signal processing, adaptive filtering, and wavelet transform.

GENNADY M. MIKHEEV received the degree and the Ph.D. degree from Moscow State University in 1981 and 1985, respectively, and the D.Sc. degree from the Russian Academy of Science in 2000.

He is currently a Professor and the Head of the Laser Laboratory, Institute of Mechanics, Udmurt Federal Research Center, Ural Branch of the Russian Academy of Sciences, Izhevsk. His research interests are focused on the interaction of laser radiation with matter.

KONSTANTIN G. MIKHEEV received the degree from the Gubkin Russian State University of Oil and Gas in 2010 and the Ph.D. degree from the Institute of Mechanics, Ural Branch of the Russian Academy of Sciences (UB RAS), Izhevsk, in 2013. He has been with the Laboratory of Laser Research Techniques since 2011. He is currently a Senior Researcher with the Institute of Mechanics, Udmurt Federal Research Center, UB RAS.

His research interests are focused on the interaction of laser radiation with carbon nanomaterials and Raman spectroscopy.

VLADIMIR I. SEMENOV received the degree in physics from I. N. Ulianov Chuvash State University, Cheboksary, Russia, in 1985, and the Ph.D. degree in optics from Ulyanovsk State Technical University, Ulyanovsk, Russia, in 2012.

Since 1999, he has been with the Department of General Physics, I. N. Ulianov Chuvash State University, where he is currently an Associate Professor. His current research interests include digital signal and image processing and continuous fast wavelet transform.